Electronics, vol. 22, no. 2, pp. 105–113, 2018

Medium Voltage Impedance-Admittance Measurement System Based on the Cascaded H-Bridge Multilevel Converter

M. Petkovic, N. Hildebrandt, F. D. Freijedo, *et al.*

POWER ELECTRONICS LABORATORY
ÉCOLE POLYTECHNIQUE FÉDÉRALE DE LAUSANNE

Medium Voltage Impedance-Admittance Measurement System Based on the Cascaded H-Bridge Multilevel Converter

Marko Petković, Nicolai Hildebrandt, Francisco D. Freijedo and Dražen Dujić

***Abstract*—Recent trends in power system design such as an increasing share of renewable energy sources and smart grids are creating different subsystem interactions that require proper investigation, understanding, describing and estimating global system stability through impedance-admittance measurement and identification. This paper proposes and presents the cascaded H-bridge multilevel inverter topology for perturbation injection converter and impedance-admittance measurement. The methodology of impedance-admittance measurement is explained together with different measurements requirements. Performance and suitability of this topology for impedance-admittance measurement is evaluated through simulations. Preliminary design principles are given for the converter. System level feasibility of the solution is proposed as a main result of the work.**

***Index Terms*—cascaded H-bridge, impedance-admittance measurement, medium voltage, system identification**

Original Research Paper
DOI: 10.7251/ELS1822105P

I. Introduction

In the wake of strong penetration of renewable energies, smart-grids and traction systems, as an example of interfacing electrical grids of different nature into traditional electrical power grids, power electronics is becoming one of the most important components of modern distributed electrical power networks. As an example, Fig. 1 shows the different components and subsystems such as solar parks, wind turbines, storage elements and different ac and dc grid interface points. More and more active loads such as power converters appear next to passive loads. Utilisation of power electronic systems inherently changes the nature of power system by introducing interactions among active components, behaviour that was not present before and is becoming increasingly complex [1], [2]. As a consequence, characterizing power systems with high penetration of power electronics is of a major interest nowadays. One of most commonly used methods to analyse the behavior and stability of a system is by characterizing small-signal impedance based models and applying the Nyquist criterion to the product between the source output impedance and load input admittance [1]–[3]. This characterization is made possible by the virtue of impedance-admittance modelling and measurement. For assessing the stability of a whole system, impedance-admittance measurement has to be performed at different nodes in the power system.

Modern complex power system may be composed of dc and ac grids of different frequencies and voltage and current levels. Stemming from this, an impedance-admittance measurement devices has to be highly modular and reconfigurable to comply with different constraints at measurement points such as system voltage and current ratings and frequency and the type of connection that can be physically made. In terms of measurements, a maximally wide possible frequency measurement range is sought for. The precision of measurements on the other side is also of utmost importance. This is due to the fact that the inclusion of switched power electronic devices, no matter how flexible, versatile and powerful in the sense of enabling the full potential of power systems, also brings some downsides such as harmonics and switching noise polluting the system voltages and currents.

The topic of impedance-admittance measurement for stability analysis of power system has established itself since last decade. In [4] an overview of impedance-admittance measurement techniques based on frequency domain identification techniques for the stability of ac systems is presented. The same work presents different practical implementations for a perturbation injection converter (PIC). Another approach is using the time-domain identification via load-stepping [5]. This method is well suitable for identification of parametrical models and its advantage is in the low number of load-stepping responses needed to identify the system. However, the drawback of this method is in the inability to characterize properly the impedances in the high-frequency range. Cross-correlation methods for extraction of small-signal impedances after injection of pseudo-random binary sequence (PRBS) are presented in [6]. Methods for measuring impedances in dq-domain using ac-sweep and wide bandwidth small-signal injection are presented in [7]–[9].

Different measurement devices are already commercially available for low-power low-voltage ranges for the design of power supplies and the technology is well-established [10]– [12]. However, medium voltage (MV) impedance-admittance measurement technology is still under development at the moment. Equipment such as programmable ac sources and grid emulators are commercial products that could be used for impedance-admittance measurement. They are designed in low voltage (LV) levels of up to 1 kV and power ratings up

Manuscript received 24 October 2018. Received in revised form 19 December 2018. Accepted for publication 20 December 2018.

The authors are with the Power Electronics Laboratory - PEL, École Polytéchnique Fédérale de Lausanne - EPFL, Station 11, CH-1015 Lausanne, Switzerland (emails: marko.petkovic@epfl.ch, nicolai.hildebrandt@epfl.ch, francisco.freijedo@epfl.ch, drazen.dujic@epfl.ch).

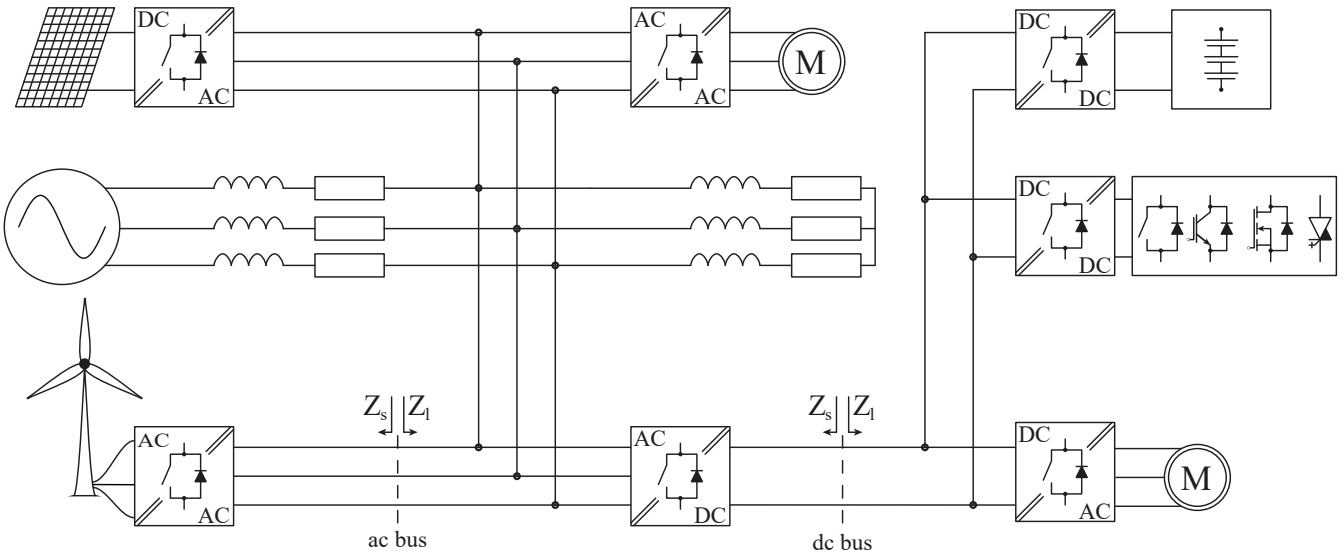

Fig. 1. Modern ac/dc distributed power system in which sources of different nature, ac or dc, and various voltage and current levels are connected through power electronics equipment. At each interface the system can be partitioned into the load and source side where each subsystem has its own characteristic impedance (or admittance) value through which the stability of the system can be assessed. Zs — source impedance, Zl — load impedance.

to 200 kVA [13]. These devices are well suited for perturbing systems as they are capable of delivering programmable harmonics or external waveform reference [13]–[16]. In general, this is a good solution when it comes to laboratory experiments at LV levels. However, from a close study in MV applications, we discarded this solution, since using this equipment for MV systems would require a step-up transformer which would in turn cause that the leakage inductances of the transformer damp the injected perturbation and thus limit the bandwidth of the PIC. This is even more noticeable at higher frequencies. The perturbation and measured signals should preferably be 10 times larger than the sensors accuracy which comes as a challenge and a target to meet. With a proper signal processing strategy this constraint could be relaxed and a set a more feasible requirement of having a measured signal that is 4 times larger than the sensor accuracy. These are known as "10:1" and "4:1" rules of thumb in metrology [17].

The previous discussion sets a motivation for our study. A complex research and design problem is established which includes topology identification and choice for PIC, as well as hardware and software design and integration. Besides, a complex measurement and data acquisition (DAQ) system has to be developed and accuracy and sensitivity to external disturbances of different sensors has to be assessed, considering noisy operational conditions. Once acquired, data has to be processed (online) or post-processed (offline). Then, in order to obtain reliable measurements, different system identification and calibration techniques can be considered. Combination of all of these elements presents itself as a perfect platform for research in medium voltage ac (MVAC) and medium voltage dc (MVDC) impedance-admittance measurements and system identification.

This work presents the selected topology for MVDC and MVAC PIC and investigates whether such a topology can be used for perturbation injection and subsequently impedance measurement. Main point of interest of this work is the terminal side and its performance potentials. The paper is organised in the following manner: Section II presents perturbation injection and measurement methods giving an overview of how the PIC can be interfaced to system. Section III presents the multilevel topology chosen and its different most important parts. Section IV presents one cell of the PIC. Section V presents relevant control aspects. Section VI presents details of the hardware design of the actual cell of the PIC. Section VII elaborates on the system foreseen for the acquisition and postprocessing of the results. Section VIII presents the simulations and performance of PIC in the environment of PIC, while the discussions and conclusion are provided in Section IX .

II. Pertubation Injection Converter and Measurement Methods

Different methods of connecting a perturbation devices to a power system to be identified have been researched and published as presented in Fig. 2. In all of these variants a small-signal perturbations, voltage or current, are injected into an unknown system, then current or voltage responses are measured and, consequently, from these the system impedance (or admittance) is identified. This work considers these three connection methods they offer a flexibility in terms of type of systems to be identified.

In the case of Fig. 2a the PIC is a main power source and an injection device at the same time, a perturbation signal is injected on top of a fundamental one. In this approach there is only one load and is well suited for grid emulators such as those in [13]–[16].

In Fig. 2b the PIC is connected in series between the source and the load subsystems and is used to inject small-signal voltage perturbations in the system. In this case the injected voltage has to be synchronized with the source voltage at the

injection point. Advantage of this method is that the power of the small-signal perturbation is low. However, this method presents itself with difficulties when it comes to PIC short-circuit protection and the PIC has to support rated system current.

Fig. 2c presents a shunt connected device between the source and load subsystems for small-signal current injection. As in the previous way, there has to exist a mean of synchronizing the injected small-

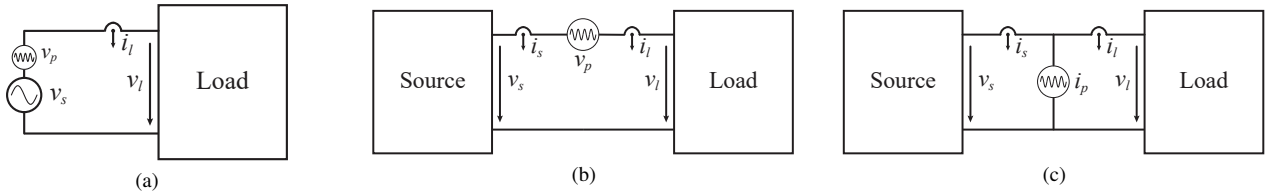

Fig. 2. Different injections methods of small signals for system identification. a) Pertubation by PIC interfacing a load and perturbing with a small voltage on top of the fundamental wave. b) Perturbation by voltage source connected in series between source and load. c) Pertubation by current source connected in shunt between source and load.

signal with the system current. Advantage of this method is that the system current does not flow through the PIC unlike with the previous method, but on the other hand the PIC has to withstand the full line voltage of the system. Current perturbation injection is better suited for identifying smaller source side impedances as often larger load side impedance will force the injected current to flow in the direction of the source, thus leaving little perturbation current for the load side and making the load side measurement and identification more difficult. Another drawback is the fact that it is difficult to inject controlled harmonic current since a closed-loop control is necessary. Connecting a device between two subsystems allows the device to be an active part of a whole system and at the same time to be a perturbation device. Methods in Fig. 2 are generic ones and present a single-phase connection. Of course, they can be extended and applied to three-phase systems which are of interest in this work.

There exists a plethora of possible signal types and waveforms that could be used for injection and system perturbation. Most basic form of perturbing a system is using the ac frequency sweep where a single frequency is injected at a time which in the large frequency range of interest makes the measurement considerably slow. Another method is to use wide bandwidth signals such as swept sine in which signal frequency increases (or decreases) over a certain time. Random signals such as PRBS is introduced as white noise approximation. Even though these signals reduce measurement time, over a large frequency range their signal-to-noise ratio (SNR) decreases making the measurement more difficult. Another suitable signal is the multisine signal which contains multiple tones at the same time. The SNR of multisine signal is constant over a frequency range but is nevertheless lower compared to a single tone signal used for the ac-sweep. Evidently, a tradeoff between the time and precision of measurement has to be made. One of the possible approaches to mitigate the problem of low SNR when using wide bandwidth signals is to use peri-odogram power spectral density methods [18], [19]. In [20] it is shown that the cross power spectral density (CPSD) estimation based on Welch periodogram spectral density estimation [21] algorithm is successfully used for identifying impedances where voltage and current measurements are affected by the noise.

When it comes to measurements themselves, in the case of Figs. 2b and 2c, source and load voltages and currents are measured while in the case of Fig. 2a, source voltage and load current are measured. Voltage and current transducers must have a sufficient accuracy. Not only magnitude but also the phase accuracy has to be high enough as the phase characteristics of sensors will also influence the impedance calculation results [7]. It goes without saying that not only high enough bandwidth is a must for these transducers, but also they need to measure reliably low-bandwidth signals. Possible candidates for transducers are voltage dividers for line voltage measurements and Rogowski and closed loop Hall current sensors for line current measurements.

Concerning voltage and current injection devices, different devices are reported in [22]–[24]. Reference [25] provides results in the MVAC grids and it describes a single phase impedance measurement unit in which three voltage source switching cells are connected in either parallel or series configuration and each of them fed from a dc-link. However, for this work, a highly scalable and modular solution, in terms of voltage and power levels, that can be employed for different applications is sought after. To this end, multilevel topologies appear as a possible candidate for the application. When directly interfacing an MV grid, multilevel converters provide a much reduced short-circuit impedance than solutions based on LV power electronics in combination with step-up transformers. We consider that cascaded H-bridge (CHB) with multiwinding transformer match a realistic / cost effective scenario. On one side these topologies are scalable and versatile. They can be used as a main source and as a perturbation source at the same time or can be used as an external device that solely serves the purposes of injecting a perturbation voltage or current. This multifunctionality can be achieved by physical reconfiguration of the converter cell connections. On the other side, in terms of control, multilevel topologies achieve a higher bandwidth (modulation and control) than topologies capable of delivering two level or three level outputs for the same output voltage and power rating. Having a higher bandwidth immediately allows higher perturbation frequencies and allows to identify the system up to a higher frequency. Thanks to the multilevel topology, there is no isolating transformer on the output side, where measurements are performed, thus no reduction in the output bandwidth that is now determined by implementation of the converter stages. Due to the advantages that this solution possesses, a multilevel CHB inverter topology supplied by a multi-winding transformer is proposed and investigated for PIC application.

III. Cascaded H-Bridge Based Impedance-Admittance Measurement Unit

Different perturbation injection devices have been reported in the literature and they suffer from one common downside, the switching noise. When the switching noise is present, together with its side harmonics it becomes much more difficult to identify system response and separate it from the noise induced by the switched operation. However, one solution to alleviate this problem, at least to some extent, is to use a CHB multilevel inverter topology. The CHB multilevel inverter topologies output waveform contain

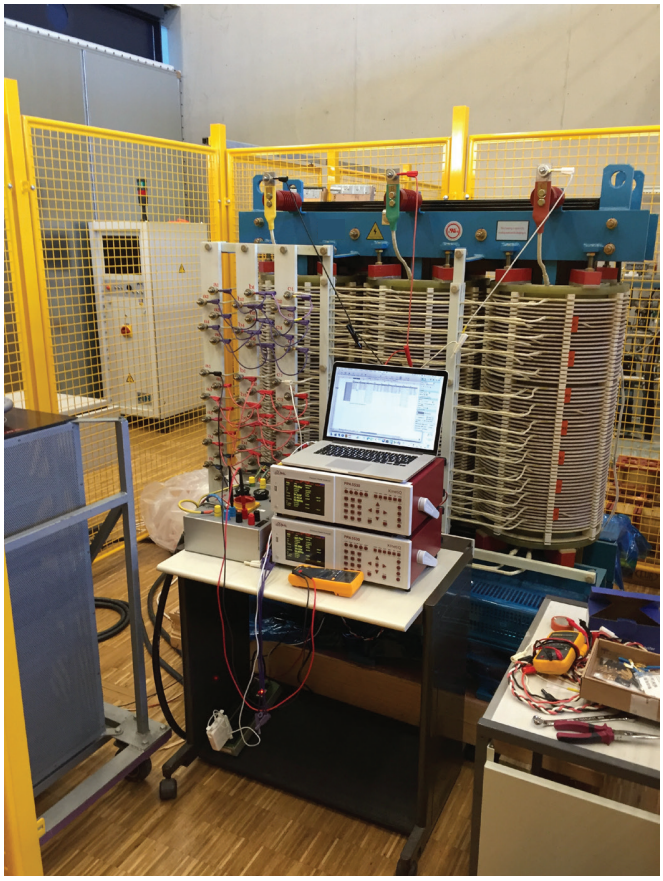

Fig. 3. 1MVA multi-winding transformer.

have lower total harmonic distortion (THD) than 2-level topologies and the harmonics are contained in high frequency range which is not of interest to us [26]. As mentioned in Section II, base for the development of this solution is the multi-winding transformer in Fig. 3. Details about the transformer characteristics and modelling for electric circuit simulations are presented in [27] and Table I. The transformer itself shall be interfaced with a multilevel CHB converter (see Fig. 4) and five secondary winding of one single phase are connected to cells which are connected in series or in parallel at the output, depending on the type of injection performed. Moreover, depending on the type of injection a different output filter is required. This results in an 11-level CHB inverter topology which is the key element of the PIC. Having such a high number of voltage levels in combination with phase-shifted carrier PWM (PSC-PWM) gives a less distorted waveform which in return gives less noise pollution and better system response to be identified.

TABLE I MULTI-WINDING TRANSFORMER PARAMETERS

Parameter	Value
Apparent Power Rating	1MVA
Primary Side Line Voltage	6.3 kV
Secondary Side Line Voltage	710 V
Grid frequency	50Hz
Star Primary Windings	1
Extended Delta Secondary Windings	15
Phase Shift of the Secondaries	-18°, -6°, 6°, 18°, 30°

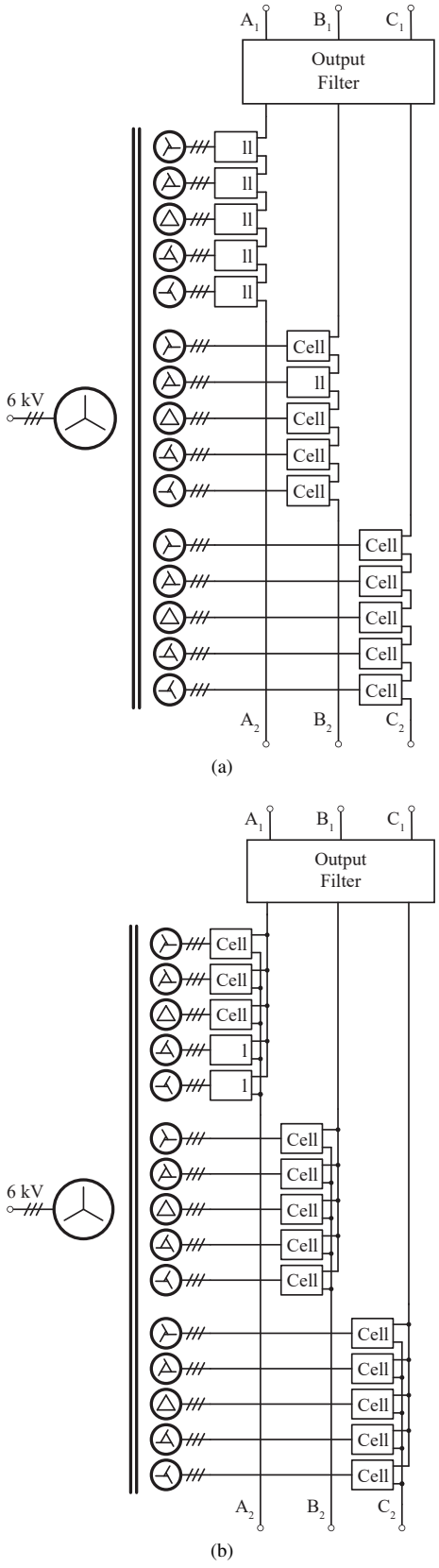

Fig. 4. CHB topology with isolated cell supply transformer with a) cell outputs connected in series for shunt current injection and b) cell outputs connected in parallel for series voltage injection.

The PIC shall be capable of providing all three connection modes as indicated in Fig. 2. In the series voltage injection mode the cells are connected in parallel, while in shunt current injection mode the cells are connected in series. As the PIC has to be connected in two different ways, the whole system has to be modular and cell connections have to be reconfigurable. The simplest and cheapest way of achieving this reconfigurability is mechanically through the system of bus bars. Most of the reported injection devices are unidirectional and are capable of creating an unidirectional perturbation whereas the topology reported in this work is a four-quadrant one and is capable of sinking current and reversing the voltage polarity which leaves open a question of influence of these methods on impedance-admittance measurement and system identification. A clear advantage is the fact that the PIC is a grid emulator and a measurement device at the same time, which allows for measurement at different grid operating points.

A. Output Waveform Filtering

The PIC is required to inject clean high-frequency small-signal voltage and current perturbations up to 10 kHz. Due to this requirement, the inverter end has to comprise a filter to eliminate the pulse-width modulation (PWM) harmonics to some extent. The inverter rectangular shaped voltages can be filtered in two ways, using the *dv/dt* and sine wave filters.

The first method filters only high frequency components to reduce the voltage slope of the PWM rectangle outputs. Since fast switching silicon carbide (SiC) MOSFETs are used to synthetize the output waveform *dv/dt* can reach high values. In any case of connection to a system seen in Fig. 2 the output voltage slope has to be limited in order not to provoke a damage to the system being identified. This requires protection equipment to be installed. The damped filter resonant frequency *fd* of this filter is chosen to be higher than both the output frequency f_{out} and the switching frequency, i.e. $f_{out} \ll f_{sw} \ll f_d$.

The second approach is used to filter out the switching frequency components to obtain a sinusoidal output waveform. Three factors determine the choice of the sinusoidal filter. The first is the tolerance of the voltage distortion level of the output filter, the second one is the maximum allowable voltage drop on the filter and the third depends on the switching frequency of the inverter switches [28]. The first two factors are directly sets the requirements on the output waveform of the PIC. Third factor reflects on the damped resonant frequency which is required to be larger than the output frequency but smaller than the switching frequency, i.e. $f_{out} \ll f_d \ll f_{sw}$.

With respect to injection methods presented in Fig. 2, the PIC may require three different output filter configurations which may result in converter loss budget savings and volume savings for both the converter and the filter. Factors that determine the choice of filter are the power losses, in the converter and the filter respectively, and voltage and current ratings that the PIC has to withstand. Two types of filters to be considered are LC and L filter (see Fig. 5). The L filter is used for the current injection, while the LC filter is used for voltage injection, i.e. L to provide a current source and LC for a voltage source. This type of output filter provides a transformerless solution at the output stage for perturbation injection. Transfer functions G_{LC}(s) and $G_L(s)$ of these filters are well known:

$$G_{LC}(s) = \frac{v_p(s)}{v_{\text{inv}}(s)} = \frac{1}{s^2 L_f C_f + 1} \tag{1}$$

$$G_L(s) = \frac{i_p(s)}{v_{\text{inv}}(s)} = \frac{1}{sL_f} \tag{2}$$

The LC filter will present a damped resonance at resonance frequency *fd,* after which all frequency components are attenuated at a rate of –40 dB/dec.

$$f_d = \frac{1}{2\pi\sqrt{L_f C_f}} \tag{3}$$

The L filter presents no resonance and acts as a first order low-pass filter with –20 dB/dec attenuation rate.

IV. Single Cascaded H-Bridge Cell

The single cell of the CHB converter is presented in Fig. 6 and it comprises an input filter, active front-end (AFE) and an H-bridge (HB) inverter. The injection converter shall be designed to support 6 kV line-to-line ac voltages and 100 A currents with up to 1MVA output power [29]. The 1MVA converter is built of 15 cells which means that each cell has a nominal power of 66.7 kVA. The PIC is required to inject only a portion of system voltage or current, namely 5-10%, in the range of 1 Hz–10 kHz. As a rule of thumb, this means that the apparent switching frequency should be 100 kHz. Since the presence of only five secondary windings per phase implies relatively low multiplication factor *(N* = 5) for the apparent

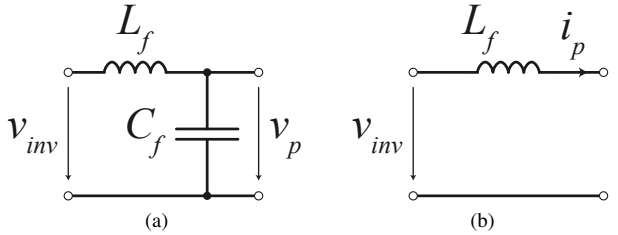

Fig. 5. a) LC and b) L output filter configuration circuits. v_{inv} — inverter ouput voltage, v_{p} — perturbation voltage, i_{p} — perturbation current.

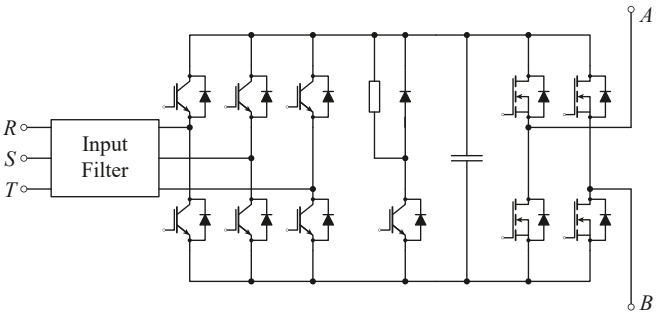

Fig. 6. Regenerative cell with an input filter, AFE stage (left) and inverter HB stage (right).

switching frequency, it means that the switches inside a HB should be switched at least at 20 kHz. Due to the high switching frequency SiC devices are considered for the HB stage [29]. Table II summarizes the cell parameters.

A. Input Filtering

As the cell is interfaced to the transformer secondary it is naturally connected to the transformer secondary leakage inductance. Following from this, different input filter configurations can be used for this application. Different options for the input filter are presented in Fig. 7. Choice of filter type and position of voltage and current transducers directly influences control strategy for the cell.

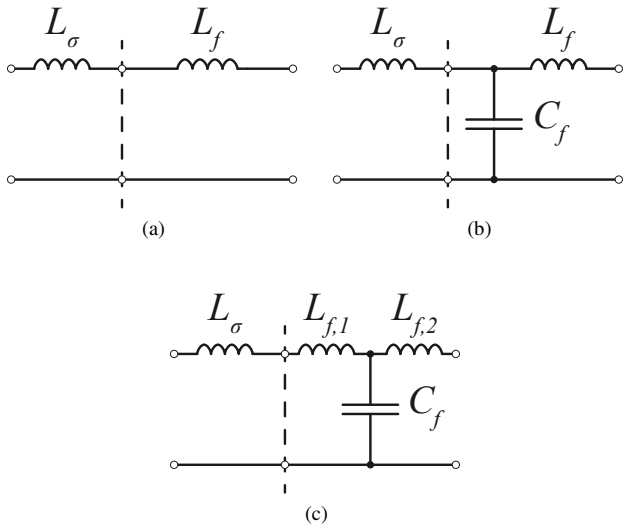

Fig. 7. Different input filter configurations: a) L input filter in combination with transformer secondary side leakage inductance forming LL filter, b) CL input filter in combination with secondary side leakage inductance forming LCL filter, c) LCL input filter in combination with secondary side leakage inductance forming LLCL filter. Dashed line represents the connection point between the transformer and input filter.

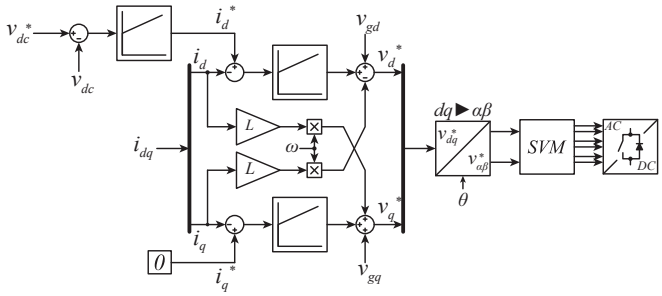

Fig. 8. AFE control diagram.

TABLE II
CELL PARAMETERS

Parameter	Value
Apparent Power Rating	66.7 kVA
AFE Nominal Current	54 A
Inverter HB Nominal Current	96 A
Nominal dc-link voltage	1200 V
Semiconductor blocking voltage	1700 V
Inverter HB Modulation	PSC-PWM

B. Active Front-End

In order to investigate the influence of having a four-quadrant topology for perturbation generation front-end is silicon IGBT based AFE. Switching frequency is set at 10 kHz. Transformer secondaries provide a multiple of 60°/N phase shift. Due to this, the current control bandwidth of AFE is rather low. On the other side, having a high dc-link voltage control bandwidth and lower filtering effort of AFE switching harmonics is sought after. This requirement is filled by increasing the AFE switching frequency. Power modules of the 1.7 kV voltage class are chosen for this application, and for simplicity reasons two-level switching cells are chosen. Reason for choosing this voltage class modules is the nominal dc-link voltage which derives from the line voltages of transformer secondaries. Package type chosen for the semiconductor module is the standard 62 mm package. This is a standard package with many alternative sources which is easy to integrate with the existing gate drivers on one hand and reduces thermal management effort on the other hand. In order to decrease the voltage overshoots due to stray inductances, a snubber capacitor rated for 1.2 kV is connected across each IGBT. Amongst many commercially available power modules, SEMIKRON SKM150GB17E4G 1.7kV IGBT power module with body diode was one of the suitable candidates for the application and was therefore chosen [29].

C. Voltage limiting circuit and dc-link

The bandwidth requirements and realization for the AFE and the HB are not the same. In case of sudden energy flow reversal and in order to prevent transient overvoltages in the dc-link, a voltage limiting circuit is also present in the cell as a protective mean. The dc-links in the cells are independent between themselves and each dc-link is controlled independently. In this way, the problem of dc-link voltage unbalance is eliminated. The purpose of the dc-link capacitor is dual. On one side it serves to maintain the desired dc-link voltage and reduce the voltage ripple, thus enabling proper dc operation point for the converter, while on the other it serves as a storage for reactive energy during low frequency injection. Unlike the usual design where low frequencies would not be considered, in this case the dc-link design needs to take into account the lowest injection frequency that needs to be achieved while at the same time taking into account the maximum allowable voltage ripple. The dc capacitor can be calculated with respect to the maximum allowed voltage ripple for the lowest injection frequency point [20]. Trying to fulfill all conditions of having highest possible small-signal voltage and current injection and lowest frequency would result in capacitance values far too big for any practical implementation which in turns forces us to make certain trade-offs, e.g. derating for lower frequency injection. For this application the dc-link nominal voltage 1200 V and the capacitance of 5 mF is set. Capacitors used for the application are film type because of high frequency injection and low output filter impedance and are rated for 1.32 kV.

D. H-Bridge Inverter

As higher switching frequencies are required at the inverter end, SiC MOSFET devices are chosen for this application. The inverter nominal current is 96 A so power modules with at least 150 A current rating are chosen. The MOSFET package is identical to the one of the

IGBT. Type of modules that will be used will be 62mm SiC 1.7kV MOSFET power modules due to the ease of integration with the AFE.

V. Control

A. Active Front End Control

There exist multiple ways of controlling the AFE unit. We have chosen that the input rectification stage and dc-link voltage are controlled by the synchronous reference frame (SRF) decoupled current control. The control diagram is presented in figure Fig. 8. i_d^*, i_q^*, i_d and i_q is the *d*- and *q*-axis current references and measurements respectively, v_g the secondary side voltage of the transformer, i_c the AFE ac input current, v_{dc}^* and v_{dc} the dc-link voltage reference and measurement. The i_d^* is obtained through the cascaded proportional-integral (PI) control of the dc-link voltage. The i_q^* is usually set to zero as there is no reactive power demand. The modulation type used is the space vector modulation (SVM). The angle θ is obtained with the SRF-phase-locked loop (PLL) by measuring primary transformer voltages and applying phase shift corresponding to each secondary.

B. CHB Multilevel Inverter Output Control

Due to the versatility requirement that multiple types of injections are possible, current or voltage ones, different control strategies can be applied for each case and these strategies directly depend on the type of output filters used. As mentioned in Subsection III-A, the LC filter is used for voltage injection, thus the voltage v_p on the capacitor is controlled, which needs to be synchronized with the system it is being injected in. In the case of current injection, the current i_p in the inductor is controlled and this current also has to be synchronized with the system current. For the injection type as the one presented in Fig. 2a, no synchronization is needed.

VI. Preliminary Hardware Construction and Prototyping

A preliminary 3D CAD representation of the cell is shown in Fig. 9. The cell layout mainly depends on the cooling system, choice of power modules packaging type, gate drivers, dc-link capacitors, snubber capacitor and insulation coordination standards that have to be respected. Due to the possible size of the input filter, it is physically placed outside the cell.

Both the AFE and HB inverter are mounted on a heatsink of the same type. This arrangement of switching devices simplifies the integration between the AFE and HB as the whole structure becomes symmetrical. This also means that the cooling system for the HB inverter is oversized for the minimal switching frequency of 20 kHz, which in turn allows for the switching frequency to be pushed even further if required. Type of heatsink used is an aluminium hollow fins heatsink which is combined with forced air cooling system. The dimensions of the heatsinks are 240 mm×120 mm×250 mm.

The copper busbar system carries the current from the input terminals through the current transducers to the power modules, the dc-link and further to the HB inverter. The current transducers are placed beneath the gate driver interface board, thus easing the connection

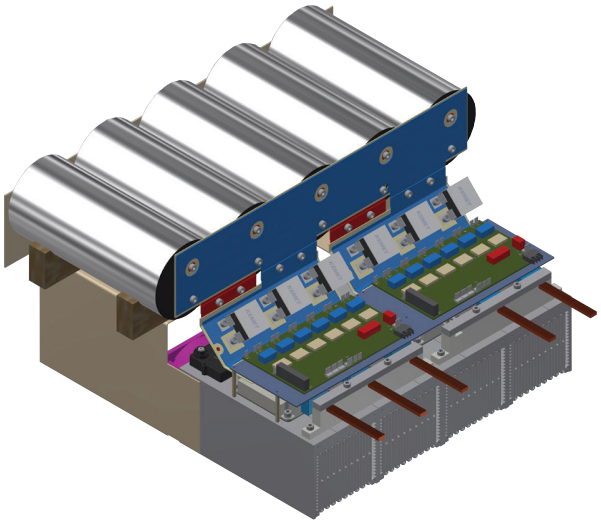

Fig. 9. 3D CAD representation of the cell. AFE is to positioned to the left side and HB inverter to the right.

to the dedicated current measurement connectors. The dc side busbars are designed as to reduce the overall stray inductance using wide parallel copper plates and aligning connections with the main current flow. The standard UL 840 is followed when designing the busbars in order to have proper creepage / clearance distances. Each dc plate is 1 mm thick which is enough to carry the nominal current. Insulating layer is made from flame retardant polypropylene electrical insulation material. The layer thickness is 30mil (0.762 mm). The dc-link is realized with five parallel film capacitors which are mounted behind the cooling system.

Gate driver circuits are placed directly on top of the power modules on their dedicated interface board as the fast switching is required and the gate signal paths should be kept as short as possible. Moreover, a metallic shielding is needed between the gate driver circuits and power modules and around the gate drivers. In this way the EMI effect on the gate drivers is reduced and it provides a physical protection of the circuits beneath.

The overall size of the system are given by two elements, dc-link and the cooling system. The overall size of the cell is 600mm×500mm×350mm. The cooling system and the dc-link account for 30 % of the overall cell volume.

VII. Measurement, Data Acquisition System and System Identification Chain

A complete system level diagram is presented in Fig. 10. It includes a PIC used for perturbation injection to an unknown system that can be composed of various components, passive and active ones, voltage and current measurements on the source and the load side, signal conditioning for DAQ instrument and finally data processing to which the system identification methods are applied.

A. Measurement system

For proper impedance identification a proper measurement system is indispensable. The measurements are implemented via voltage and current sensors placed on the source and on the load side. Both the line-to-line voltages and currents are measured. Due to the maximum

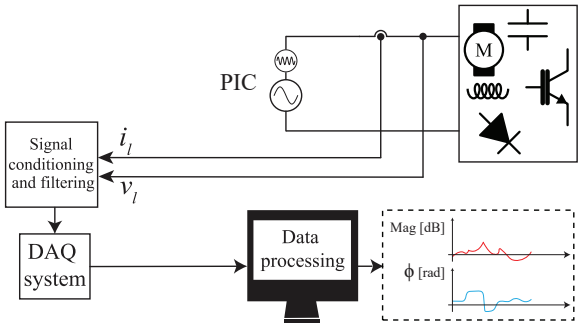

Fig. 10. Complete system block diagram.

injection frequency sought for, voltage and currents up to 10 kHz need to be measured at the MV level. Measurement devices need to measure the full range voltages and currents while having a constant gain and almost no phase delay in the frequency range of interest, otherwise it will affect the computed impedance value. Moreover, each measurement has to be conditioned, i.e. filtered and scaled for the DAQ instrument, for which a dedicated measurement conditioning system needs to be designed. The challenge regarding the sensor design is the fact that they need to measure the full range quantities, even though only the perturbation portion is of interest in the end.

B. Data Acquisition System

Next step is feeding the conditioned measurement to DAQ instrument. The DAQ system needs to be equipped with enough acquisition channels to acquire synchronously all voltage and current measurements needed. In the DAQ instruments, the analog measurements are sampled using a high enough sampling rate and converted to their digital counterparts.

C. Data Processing and System Identification

Final step in the chain is the data processing and application of system identification methods in order to compute the impedance. The signal processing is performed in an external PC and relies on the methods such as those in [20]. Another important part in the chain is the visualization of results over the full frequency range.

VIII. Perturbation Injection Converter Performance

Three different configurations presented in Fig. 2 were simulated. PIC is connected to a load of i?$_{load}$ = 36 *Cl* and Lload = lmH. Fundamental output line-to-line voltage is 5.4 kV and small-signal voltage is 600 V, i.e. 10% of maximum line-to-line voltage. In this configuration power output of the PIC is 1 MW.

Fig. 11 presents results for the case in which the PIC is the main source and perturbation source, as in Fig. 2a.

Fig. 12 presents load voltage and currents in the case where the small-signal voltage perturbation is injected in series with a source between the source and the load, as in Fig. 2b. Again, the source voltage is 5.4 kV while the small-signal voltage is 600 V and the load characteristic is the same.

Fig. 13 presents source voltage and currents in the case where the current perturbation is injected in shunt at a point between the source and the load, as in Fig. 2c. In this case the source voltage is 6 kV and the load characteristic is the same. Current injected by the PIC is 9.6 A. In all three configurations perturbations at 1 Hz, 1 kHz and 10 kHz are injected.

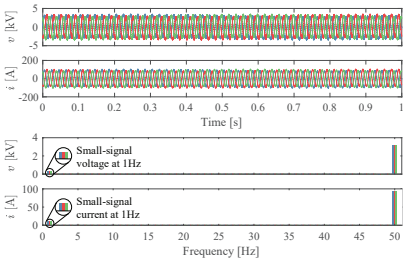

(a) Case of a 1 Hz source voltage injection on top of a 50 Hz fundamental wave

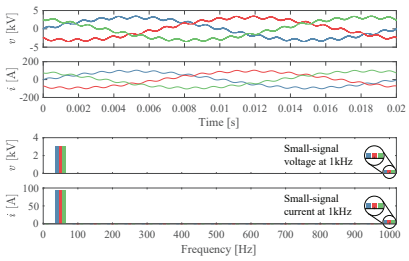

(b) Case of a 1 kHz source voltage injection on top of a 50 Hz fundamental wave

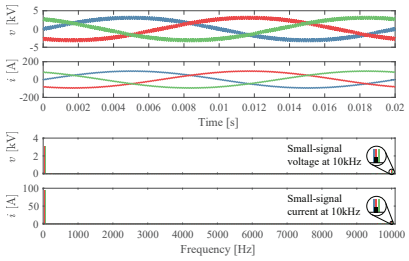

(c) Case of a 10 kHz source voltage injection on top of a 50 Hz fundamental wave

Fig. 11. Simulation waveforms for the configuration in Fig. 2a. a, b and c phase voltages and currents are visible in blue, red and green.

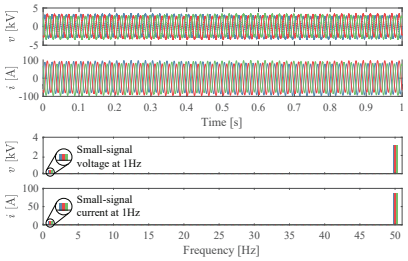

(a) Case of a 1 Hz source voltage injection on top of a 50 Hz fundamental wave

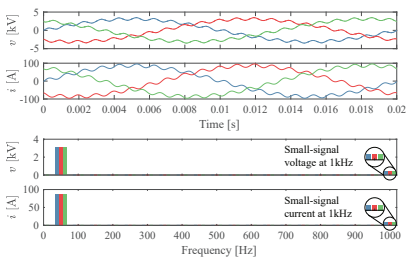

(b) Case of a 1 kHz source voltage injection on top of a 50 Hz fundamental wave

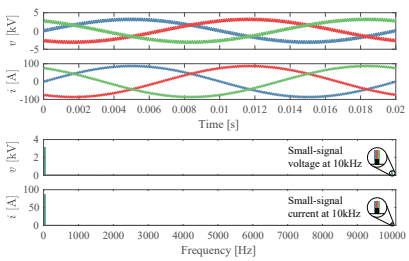

(c) Case of a 10 kHz source voltage injection on top of a 50 Hz fundamental wave

Fig. 12. Load side simulation waveforms for the configuration in Fig. 2b. a, b and c phase voltages and currents are visible in blue, red and green.

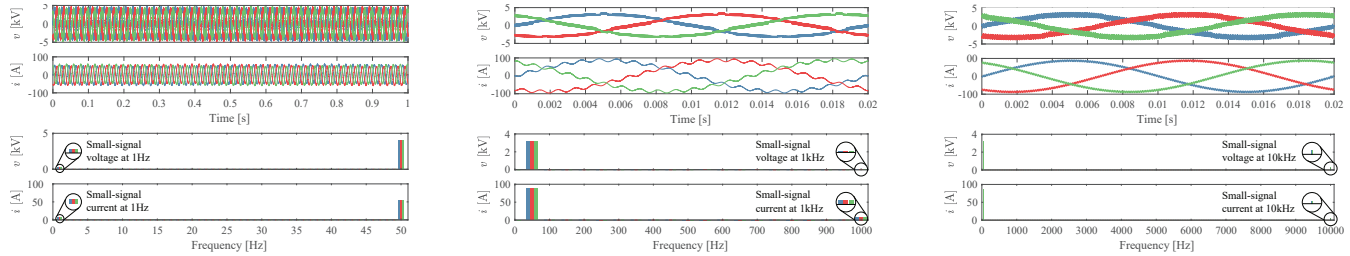

(a) Case of a 1 Hz source voltage injection on top of a 50 Hz fundamental wave

(b) Case of a 1 kHz source voltage injection on top of a 50 Hz fundamental wave

(c) Case of a 10 kHz source voltage injection on top of a 50 Hz fundamental wave

Fig. 13. Source side simulation waveforms for the configuration in Fig. 2c. a, b and c phase voltages and currents are visible blue, red and green.

IX. Conclusion

This paper focused on the CHB topology employed as a PIC whose objective usage is impedance-admittance measurement and system identification. The use of multilevel topology in combination with fast switching devices allows higher apparent switching frequencies and consecutively high frequency output voltage and current which also means a higher bandwidth and better system characterization. Moreover, versatility of the proposed solution provides a capability of having a main source and a perturbation source in the same device, a possibility of connecting the device in three different configurations at various interfaces in the system. Owing to the scalability, the proposed topology can be used at different voltage and current levels.

References

[1] X. Wang and F. Blaabjerg, "Harmonic stability in power electronic based power systems: Concept, modeling, and analysis," IEEE Transactions on Smart Grid, pp. 1–1, 2018.

[2] U. Javaid, F. D. Freijedo, D. Dujic, and W. Van Der Merwe, "Dynamic assessment of source–load interactions in marine MVDC distribution," IEEE Transactions on Industrial Electronics, vol. 64, no. 6, pp. 4372– 4381, 2017.

[3] R. D. Middlebrook, "Input filter considerations in design and application of switching regulators," IEEE Industry Applications Society Annual Meeting, 1976.

[4] Y. A. Familiant, J. Huang, K. A. Corzine, and M. Belkhayat, "New techniques for measuring impedance characteristics of three-phase ac power systems," IEEE Transactions on Power Electronics, vol. 24, no. 7, pp. 1802–1810, 2009.

[5] V. Valdivia, A. Lázaro, A. Barrado, P. Zumel, C. Fernández, and M. Sanz, "Impedance identification procedure of three-phase balanced voltage source inverters based on transient response measurements," IEEE Transactions on Power Electronics, vol. 26, no. 12, pp. 3810– 3816, Dec. 2011.

[6] D. Martin, E. Santi, and A. Barkley, "Wide bandwidth system identification of ac system impedances by applying pertubations to an existing converter," in Energy Conversion Congress and Exposition (ECCE), 2011 IEEE, IEEE, 2011, pp. 2549–2556. [7] G. Francis, "An algorithm and system for measuring impedance in dq coordinates," PhD thesis, Virginia Polytechnic Institute and State University, 2010. [8] Z. Shen, "Online measurement of three-phase ac power system impedance in synchronous coordinates," PhD thesis, Virginia Polytechnic Institute and State University, 2013.

[9] G. Francis, R. Burgos, D. Boroyevich, F. Wang, S. Zhiyu, P. Mattavelli, K. Karimi, and S.-w. J. Fu, Algorithm and implementation system for measuring impedance in the dq domain, US Patent 9,140,731, Sep. 2015.

[10] Ridley Engineering. (2016). AP300 Analyzer, [Online]. Available: http: //old.ridleyengineering.com/analyzer.html.

[11] Omicron Lab. (2017). Fast and easy measurements with the Bode 100, [Online]. Available: https://www.omicron-lab.com/bode-100/product-description.html.

[12] Keysight Technologies. (2018). Impedance Analyzers, [Online]. Available: https://www.keysight.com/en/pc-1000000382%3Aepsg%3Apgr/ impedance-analyzers?cc=US&lc=eng.

[13] EGSTON, COMPISO P-HIL System, https://egston.com/01-power-electronics/?lang=en.

[14] Regatron, TopCon TC.ACS - Full 4-quadrant grid simulator, https : //www.regatron. com/en /products-topcon/ 18- english-categories / products/94-topcon-tc-acs-full-4-quadrant-grid-simulator.

[15] Cinergia, GE - Grid Emulator series, http : //www. cinergia.coop / cinergia-product/ge-grid-emulator-series.

[16] Spitzberger and Spies. (2012). PAS series of 4-Quadrant Amplifi ers, [Online]. Available: www . spitzenberger . de / download . ashx ? weblink=1002.

[17] RFM. (2017). Ten to One or One to Ten Rule, [Online]. Available: https://rfminc.net/resource-center/metrology-tips/ten-to-one-to-ten/.

[18] M. K. Steven et al., "Modern spectral estimation: Theory and application," Signal Processing Series, 1988.

[19] P. Stoica, R. L. Moses, et al., Spectral analysis of signals. Pearson Prentice Hall Upper Saddle River, NJ, 2005, vol. 1, pp. 22–55.

[20] M. D. Jaksic, "Identification of small-signal dq impedances of power electronics converters via single-phase wide-bandwidth injection," PhD thesis, Virginia Polytechnic Institute and State University, 2015.

[21] P. Welch, "The use of fast fourier transform for the estimation of power spectra: A method based on time averaging over short, modified periodograms," IEEE Transactions on audio and electroacoustics, vol. 15, no. 2, pp. 70–73, 1967.

[22] Y. L. Familiant, K. A. Corzine, J. Huang, and M. Belkhayat, "Ac impedance measurement techniques," in IEEE International Conference on Electric Machines and Drives, 2005., May 2005, pp. 1850– 1857.

[23] M. Jaksic, Z. Shen, I. Cvetkovic, D. Boroyevich, R. Burgos, and P. Mattavelli, "Wide-bandwidth identification of small-signal dq impedances of ac power systems via single-phase series voltage injection," in 17th European Conference on Power Electronics and Applications (EPE'15 ECCE-Europe), Sep. 2015, pp. 1–10.

[24] Z. Shen, M. Jaksic, P. Mattavelli, D. Boroyevich, J. Verhulst, and M. Belkhayat, "Three-phase ac system impedance measurement unit (IMU) using chirp signal injection," in 2013 Twenty-Eighth Annual IEEE Applied Power Electronics Conference and Exposition (APEC), Mar. 2013, pp. 2666–2673.

[25] M. Jakšić, Z. Shen, I. Cvetković, D. Boroyevich, R. Burgos, C. Di-Marino, and F. Chen, "Medium-voltage impedance measurement unit for assessing the system stability of electric ships," IEEE Transactions on Energy Conversion, vol. 32, no. 2, pp. 829–841, Jun. 2017.

[26] D. Grahame Holmes and Thomas A. Lipo, "Carrier Based PWM of Multilevel Inverters," in Pulse Width Modulation for Power Converters: Principles and Practice. IEEE, 2003, pp. 452–464.

[27] M. Luo, D. Dujic, and J. Allmeling, "Leakage flux modeling of medium-voltage phase-shift transformers for system-level simulations," IEEE Transactions on Power Electronics, pp. 1–1, 2018, (early access).

[28] J. Guzinski, H. Abu-Rub, and P. Strankowski, Variable speed AC drives with inverter output filters. John Wiley & Sons, 2015, pp. 65–93.

[29] N. Hildebrandt, M. Petković, and D. Dujić, "Evaluation of 1.7 kV SiC MOSFETs for a regenerative cascaded H-bridge multilevel converter cell," in 2018 IEEE International Conference on Industrial Technology (ICIT), Feb. 2018, pp. 718–723.